Schiff Base-Decorated Graphene Oxide as Corrosion Inhibitor for Carbon Steel Type C1025 in Acidic Solution

Ali Abra Naser*

Ministry of Education-General Directorate of Misan Education, Al-Hussein District, Al-Shabaka Street, Al-Majir Al-Kabeer, Misan 62001, Iraq

** **Corresponding author:***

tel: +964-7710498865
email: aabra0595@gmail.com

Received: April 13, 2025
Accepted: June 26, 2025

DOI: 10.22146/ijc.105964

Abstract: *Schiff-base functionalized graphene oxide (GOPT) has garnered significant attention due to its unique properties and promising applications in several fields. The synthesized compounds were characterized using various methods, including Raman shift, FTIR, XRD, EDS, and FESEM. Using the Tafel technique, GOPT was evaluated as a corrosion inhibitor for alloy (C1025) at various temperatures in an acidic solution containing 0.1 M HCl. According to the data, the inhibition of the efficiency of GOPT at 15 ppm concentration at 298 K is 88.6%. Studies on the influence of temperature on the corrosion process between 298 and 308 K showed that efficiency increased with temperature. Activation energy, activation enthalpy, Gibbs free energy of activation, activation entropy, adsorption enthalpy, adsorption entropy, free energy of adsorption, and equilibrium constant were calculated as kinetic and thermodynamic parameters. The adsorption was physically based on the activation energy, and the process was endothermic, as indicated by the enthalpy values. The Gibbs free energy values also determine the inhibitor's effectiveness in reducing alloy corrosion. GOPT produces a Langmuir adsorption isotherm with an R^2 value of approximately 0.95. These results confirm that the GOPT is a good corrosion inhibitor with potential for use in industrial applications requiring protection.*

Keywords: *graphene oxide; Schiff base; corrosion; carbon steel; acidic solution*

■ INTRODUCTION

One of the most important chemical processes that compromises metals' mechanical and structural integrity is corrosion, especially in acidic conditions in industrial settings like power plants, refineries, and chemical production facilities [1]. Carbon steel pipes are often employed in these settings because of their advantageous qualities and affordable price. However, their significant vulnerability to corrosion severely limits their operating longevity and dependability [2]. Effective corrosion inhibitors must thus be developed and put into use immediately to prolong the helpful life of metallic components and lessen corrosion-related damage [3-4]. Conventional corrosion inhibitors nevertheless confront several difficulties despite much study and use, particularly in acidic conditions where metals are prone to chronic deterioration [5-6]. The extensive industrial use of these inhibitors is hampered by problems, including ongoing material degradation, inhibitor instability in changing environmental circumstances (such as high temperatures and changing acid concentrations), and expensive material prices [7-9].

Its special qualities, including its high surface area and mobility, are key features because they increase surface coverage and inhibitor distribution, improving corrosion resistance. Many functional groups, such as graphene oxide (GO), have garnered much interest from the scientific community in recent years. Because of these characteristics, GO is a material that shows promise for a wide range of technological applications [10-11]. Organic substances like Schiff bases may be chemically added to GO for highly effective corrosion inhibitors [12-13]. Schiff base compounds are highly effective at adhering to metal surfaces and creating

protective coatings that reduce the metal's contact with its corrosive surroundings [14-16]. Schiff bases have attracted interest owing to their improved protective properties, simple synthesis from inexpensive precursors, and environmental sustainability. These compounds possess an azomethine (C=N) group, which enhances their effectiveness as inhibitors. The condensation of an aldehyde or a ketone with an amine in the presence of an acid forms Schiff bases. Thus, organic compounds containing π-electron-donating functional groups have good and distinctive properties to prevent corrosion [17-18].

The aim of this study is to explore innovative solutions to the corrosion problem through the synthesis of GO composites with Schiff bases. These hybrid materials exhibit distinct physical and chemical characteristics, enabling them to interact effectively with metal surfaces. The modification of GO with Schiff base compounds—containing nitrogen and oxygen donor atoms—enhances their ability to bind with carbon steel surfaces. This interaction results in forming a stable, adherent protective layer that improves corrosion inhibition efficiency. The performance of the synthesized inhibitor will be evaluated using electrochemical techniques, which will contribute to a deeper understanding of the inhibition mechanism and the effectiveness of the proposed corrosion inhibitor.

■ EXPERIMENTAL SECTION

Materials

In this study, chemicals were purchased from different sources as follows: dimethylformamide (DMF, 99%, Merck), *N*,*N*'-dicyclohexylcarbodiimide (DCC, 99.94%, Bide Pharmatech Ltd), 4-hydroxybenzaldehyde (98%, Sigma Aldrich), 4-dimethylaminopyridine (DMAP, 99.15%, Shanghai Chemical Technology), ethylenediamine (99%, Sigma Aldrich), Hydrochloric acid (HCl, 37%, B.D.H), ethanol (99% VWR), and chemical composition of carbon steel alloy C1025 are shown in Table 1.

Instrumentation

This study employed a comprehensive suite of analytical instruments to characterize the samples. Fourier-transform infrared (FTIR) spectroscopy was conducted using a Shimadzu FTIR-8400S spectrometer (Tokyo, Japan) with the KBr disc method. Spectral data were collected over the range of 400 to 4000 cm^{-1} with a spatial resolution of 4 cm^{-1} across 100 scans. Raman spectroscopy was performed using a portable Renishaw Raman analyzer (UK) equipped with a 532 nm excitation laser, capable of recording spectra within the 0–5000 cm^{-1} range at an average spectral resolution of 5 cm^{-1}. The spectral data were subsequently processed using Origin Lab software. Elemental composition was assessed via energy-dispersive X-ray spectroscopy (EDX) using a Bruker xFlash6i10 system operated at 0–20 kV. Morphological analysis was conducted with a field emission scanning electron microscope (FESEM), specifically the FEI Nova NanoSEM450, which offers magnification from 20× to 5000× and an accelerating voltage of 15 kV. Finally, crystallographic information was obtained through X-ray diffraction (XRD) analysis using a Rigaku diffractometer equipped with Ni-filtered Cu Kα radiation (λ = 0.15406 nm).

Procedure

The prepared Schiff base of GO

The modified Hummers method is the most common GO synthesis procedure. Graphite is oxidized using potassium permanganate and strong acids such as sulfuric acid. Three stages are involved in the synthesis of GO with *p*-hydroxybenzaldehyde and ethylenediamine (GOPT). Initially, the GO with *p*-hydroxybenzaldehyde (GOP) was formed by sonicating 0.5 g of GO for 30 min in 50 mL of DMF. Subsequently, 4-hydroxybenzaldehyde (1.22 g, 10 mmol) was added and

Table 1. Chemical composition of carbon steel

Alloy	Composition										
Carbon steel (C1025)	C	P	S	Cr	Ni	Mn	Si	As	Cu	other	Fe
	0.27	0.003	0.002	0.029	0.008	0.69	0.2	0.15	0.038	0.1249	Balance

dispersed using sonication for 30 min. The reaction mixture was further supplemented with DCC (2.6 g, 10 mmol) and DMAP (1.22 g, 10 mmol) in succession. The mixture was stirred for 4 h at 25 °C. The second step is to establish the GOP functional group. The reaction mixture was neutralized with 5% HCl, cooled to room temperature, and then ethylenediamine (0.7 mL, 10 mmol) was added and dispersed using sonication for 1 h. Subsequently, 100 mL of ethanol had been added. The mixture was refluxed for four hours to facilitate the production of the GOPT compound. The process of purification is the third stage. After filtering, the raw material was repeatedly washed with distilled water and ethanol. The purified material was dried in a vacuum oven at 60 °C for 24 h. Ultimately, the purified product was collected and stored in a desiccator until further analysis [18-19].

Schemes 1 and 2 refer to the compound prepared for this study. Water molecules were produced in this ester reaction between GO and *p*-hydroxybenzaldehyde when both substances' carboxyl group of GO and the hydroxide group interacted. The reaction is indicated by a red circle that illustrates the chemical response in Scheme 1 [18-19]. Following the elimination of water molecules, the aldehyde group of the substance (GOP) reacted with the amine group of the product ethylene diamine to form a Schiff base, which is a C=N bond (GOPT). A red circle in the chemical structure was used to indicate the reaction of this produced molecule, which is regarded as novel in Scheme 2 [20-21].

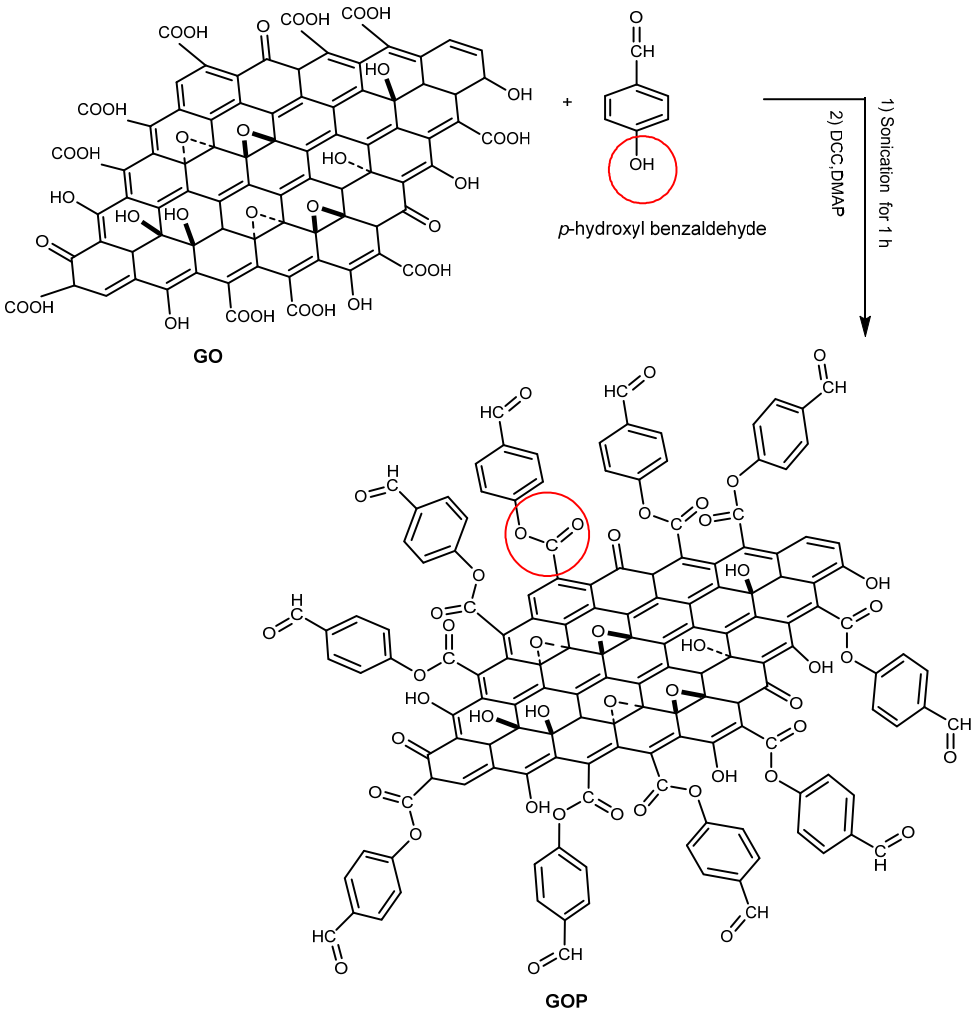

Scheme 1. The synthesis of GOP

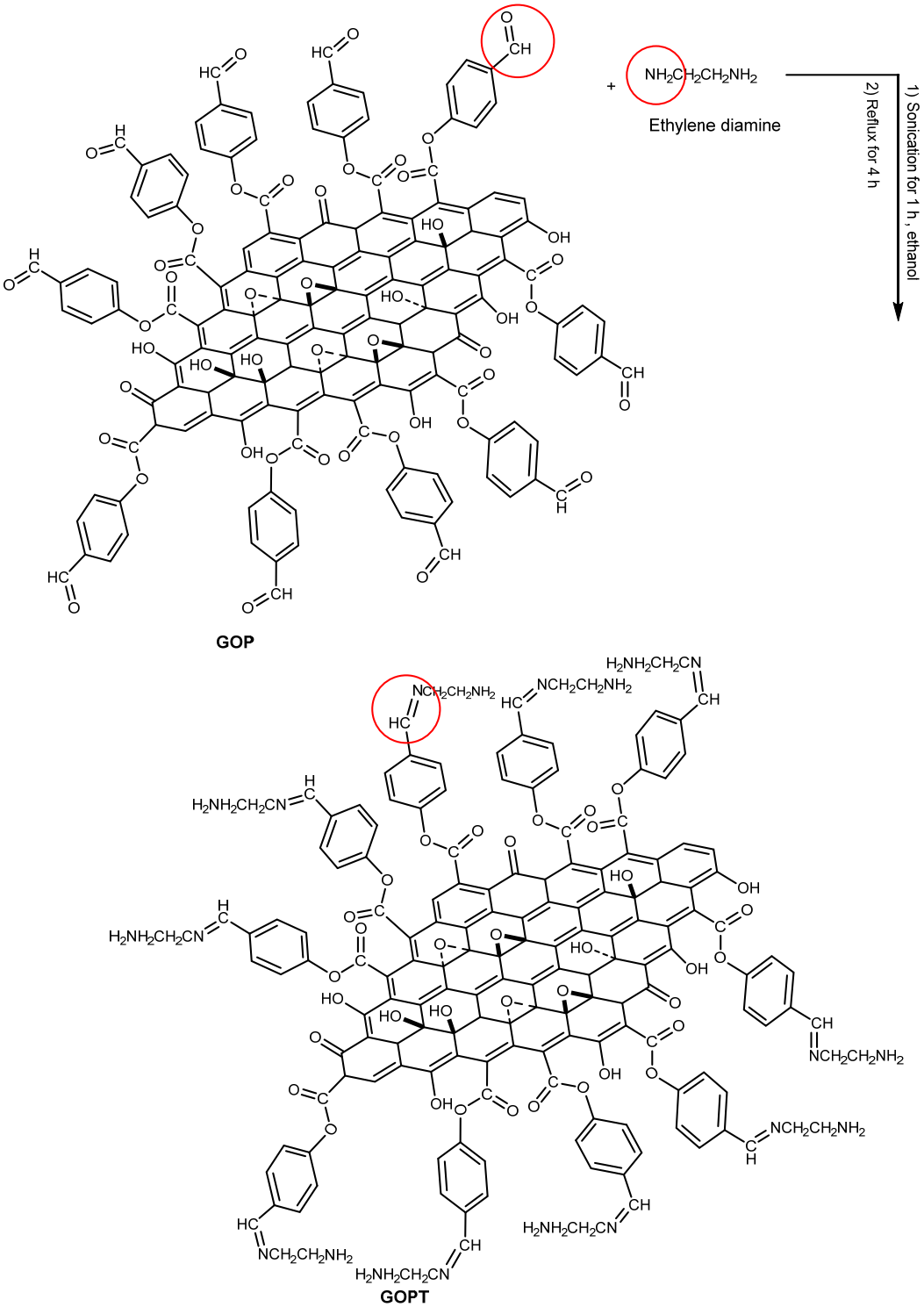

Scheme 2. The synthesis of GOPT

Preparation of functional electrodes and solutions

Strips of carbon steel alloy (C1025) were used, 2 cm long, 2.55 cm wide, and 0.35 cm thick. The total surface area of the strips was 12.4925 cm^2. Initially, silicon carbide paper with increasingly larger grit sizes (80, 120, 200, 400, and 600) was employed to etch the strips. They

were cleaned with distilled water, ethanol, and acetone before being submerged in the test liquid. They were then dried and kept dry in a desiccator with silica gel. On the other hand, 0.1 M of HCl was used to make the compound (corrosive medium) synthesized independently at various concentrations (3, 6, 9, 12, and 15 ppm) and temperatures (298, 308, 318, and 328 K).

Tafel plot (potentiodynamic studies) and electrochemical cells

This method, which measures corrosion current density (I_{corr}) versus electric potential, is frequently used to measure corrosion resistance and other parameters. First, 20 min were allotted for the open-circuit potential (OCP) setting. Utilizing a computer-controlled potentiostat/galvanostat with a sweep, the polarization curve was acquired, spanning the potential range of −250 to +250 mV (with respect to the OCP) at a rate of 1 mV/s. In the study, corrosion was examined using an electrochemical cell. To create the cell, three electrodes were attached to a 100 mL beaker in the following configuration: The reference electrode was a saturated calomel electrode (SCE), the working electrode was a carbon steel sample, and the counter electrode was a platinum electrode.

The inhibitor efficiency (%E) and surface coverage (θ) are calculated based on values of corrosion rate (CR) by Eq. (1) and (2) [22];

$$IE\% = \frac{CR_{unhib} - CR_{inhib}}{CR_{unhib}} \times 100\% \quad (1)$$

$$IE\% = \theta \times 100\% \quad (2)$$

where CR_{unhib} and CR_{inhib} denote the corrosion rates in inhibited and uninhibited systems, and IE% represents the inhibitor efficiency [23]. By calculating the kinetic parameters of Gibbs free energy, using carbon steel alloys with and without inhibitors at varying concentrations (3, 6, 9, 12, and 15 ppm), Table 1 was used to analyze how temperature affected the CR, Gibbs free energy of activation (ΔG*), activation enthalpy (ΔH*), activation entropy (ΔS*) and activation energy (E_a). To calculate the E_a value, the Arrhenius equation in Eq. (3) can be used [24];

$$\ln CR = \ln A - \frac{E_a}{RT} \quad (3)$$

where T = temperature (K), A = Arrhenius pre-exponential constant, and R = gas molar constant (8.3143 J/K.mol). Plotting ln CR vs. 1/T using Eq. (3), where the slope = $-E_a/R$ and the intercept equals ln A. On the other hand, Eq. (4) was used to compute the ΔS* and ΔH*. In contrast, Eq. (5) was used to derive ΔG* [25];

$$\ln\frac{CR}{T} = \ln\frac{R}{Nh} + \left(\frac{\Delta S^*}{R}\right) - \left(\frac{\Delta H^*}{RT}\right) \quad (4)$$

$$\Delta G^* = \Delta H^* - T\Delta S^* \quad (5)$$

where h is Planck's constant (6.62×10^{-34} JS) and N is Avogadro's constant (6.022×10^{23} mol^{-1}).

■ RESULTS AND DISCUSSION

The FESEM images of GO and GOPT reveal relatively uniform nanosheet morphology, with no apparent large-scale aggregation or structural defects. However, some surface variations and wrinkling are visible at the nanoscale. As shown in Fig. 1(a) that GO surface contains kinked areas and several layers of light grey. Buds were seen on a smooth surface in the GO image. While observing in Fig. 1(b), GOPT revealed solid

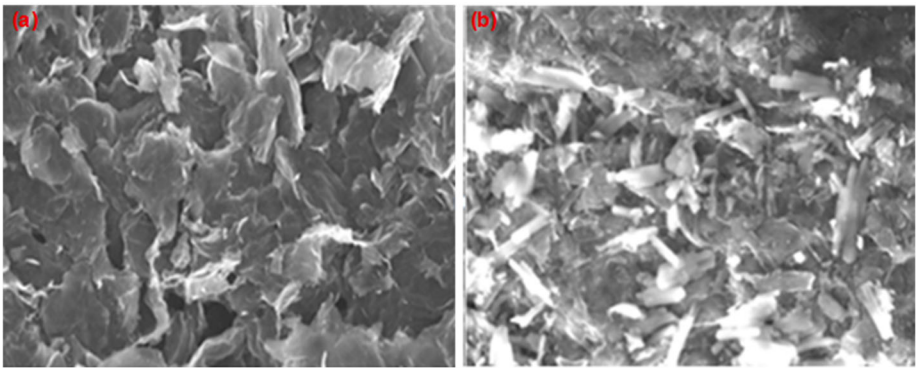

Fig 1. FESEM image for (a) GO and (b) GOPT

crumbs on porous surfaces. GOPT displayed a scattered, rough surface stuffed with macrospores, showing that the chemical change on the GO surface had been successfully modified [26].

The EDX study provides a thorough chemical analysis of the GO surface. The literature showed that Carbon and oxygen comprised most of the GO [19]. After nitrogen was added to the synthesized Schiff base compound on the GO surface, elemental mapping using EDX was done to understand the distribution of the compound on the surface. According to the elemental mapping, nitrogen was uniformly distributed over the GO surface (Fig. 2 and 3 and Table 2). According to EDX measurements, two additional peaks in the generated compound demonstrate that glass was utilized as the surface [27].

In the Raman spectra of GO, two main bands are typically observed: G band (~1602 cm^{-1}): This band corresponds to the in-plane vibration of sp^2-bonded carbon atoms. It is associated with the graphitic (ordered) structure. D band (~1359 cm^{-1}): This band arises due to defects and disorder in the carbon lattice, such as edges, functional groups, or sp^3 hybridized carbon atoms. The presence of the D and G bands in the GOPT sample (Fig. 4) at 1372.8 and 1588.9 cm^{-1}, respectively, indicates that the material still contains a similar carbon structure to that of GO, with both ordered (sp^2) and disordered (sp^3 or defective) regions. The slight shift in the band positions can be explained by: Structural or chemical modifications during the preparation of GOPT, a change in the level of oxidation or reduction, Strain or stress within the carbon lattice, and functionalization or interaction with other molecules. In summary, the D and G bands are characteristic features of carbon-based materials [17].

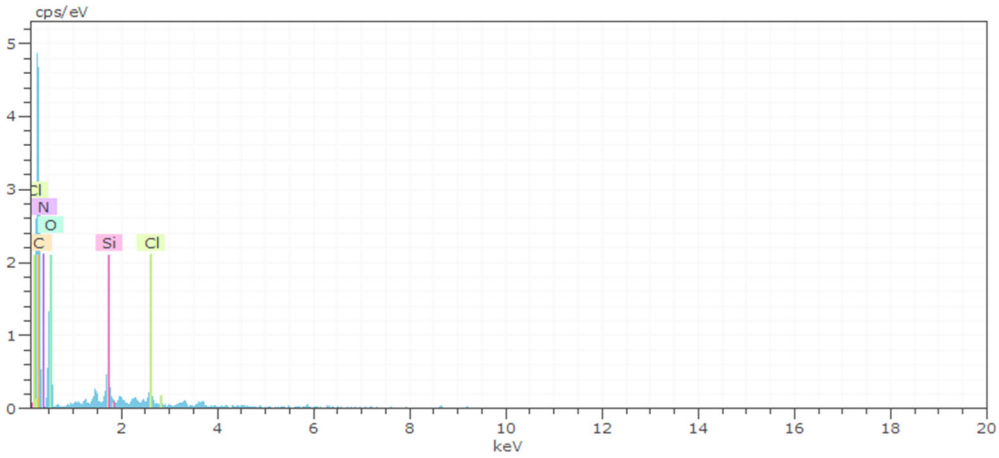

Fig 2. EDX spectra and elemental analysis for GOPT

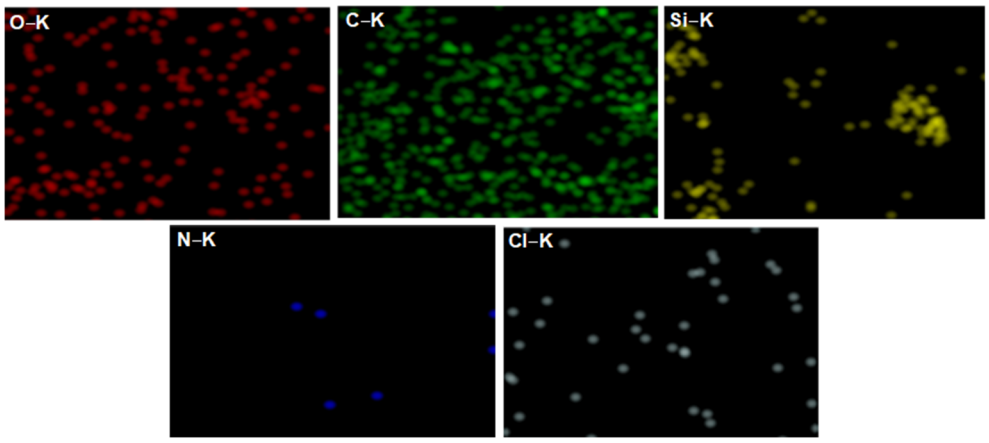

Fig 3. Elemental mapping for GOPT

Table 2. EDX spectra data for GOPT

Element	AN.	Series	Kev	Norm.wt. %	Norm.at. %
C	6	K-series	11.45	61.17	68.04
O	8	K-series	8.81	34.17	28.53
N	7	K-series	2.88	2.71	2.58
Si	14	K-series	0.12	1.10	0.53
Cl	17	K-series	0.11	0.84	0.32

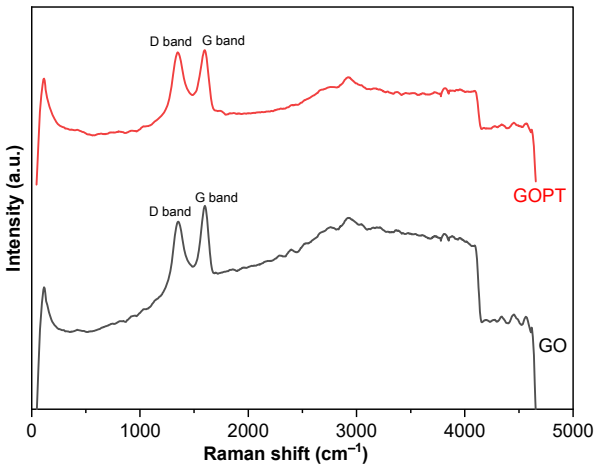

Fig 4. Raman shift for GO and GOPT

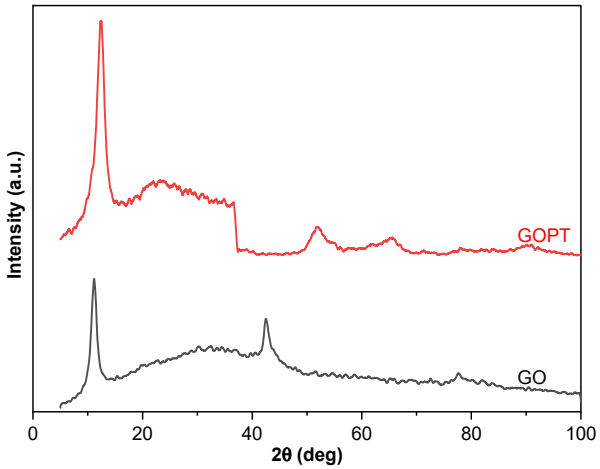

Fig 5. XRD patterns for GO and GOPT

Their presence in GOPT confirms that it retains the key structural features of GO, while the shifts suggest some changes in bonding or structural order. In contrast to GO (I_D/I_G = 0.90), GOPT had a higher I_D/I_G ratio (0.98), which resulted in a successful chemical alteration on the GO surface to create GOPT.

XRD data for GO and GOPT were analyzed using Origin software. In Fig. 5, the central diffraction peak for GO appeared at $2\theta \approx 11.15°$. This finding aligns with those reported in previous studies [19,28]. The calculated interlayer spacing was approximately 0.8 nm for GO. While GOPT, the central peak shifted to $2\theta \approx 12.35°$, indicating a reduced interlayer spacing of 0.72 nm due to the removal of oxygen-containing functional groups and increasing peak intensity. This means that the GOPT compound was synthesized through a successful chemical modification of GO [29-30].

The FTIR spectra of GOPT and GO are contrasted in Fig. 6. A massive peak at 3350 cm^{-1} is produced by the stretching of O–H (hydroxyl and carboxylic acid) bonds [31-32] on the GO surface, while a peak at 1728.28 cm^{-1} is produced by the carbonyl groups on the GO's outer border.

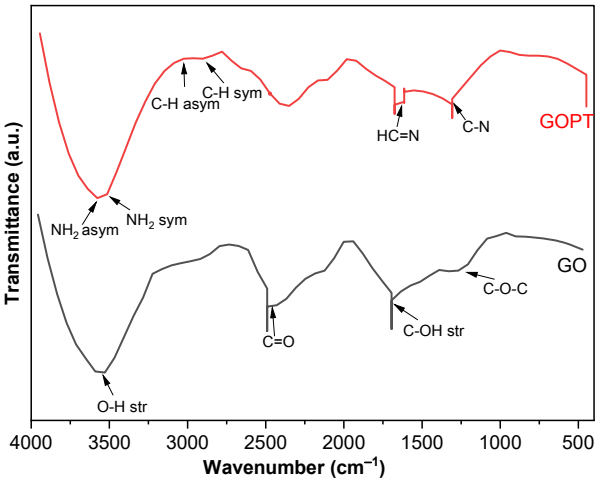

Fig 6. FTIR spectra for GO and GOPT

The presence of aromatic rings, C–OH, and C–O–C bonds in the GO structure is confirmed by the peaks at 1408, 1219, and 1051 cm^{-1}, respectively. The prominent peaks at about 3550 and 3520 cm^{-1} are due to N–H stretching vibrations, while the smaller peaks at 3047 and 2918 cm^{-1} are due to C–H stretching vibrations. The peak in the second FTIR spectra at 1630 cm^{-1} is associated with the GO functionalization in GOPT [33-34].

It was observed that the compound GOPT's polarization resistance (Rp), surface coverage (θ), and inhibition efficiency (%E) all increased with the inhibitor's concentration throughout all temperatures and concentrations, as indicated in Table 3. The Rp value rises due to some inhibitors adhering to the alloy's metal surface and creating a barrier against the corrosive environment. Because of the formation and adsorption of the inhibitor protection layer of GOPT on the metal surface, the corrosion current density (I_{corr}) values in the presence of inhibitors were lower than those in their absence at all concentrations and temperatures. As a result, there is significant electrical resistance on the alloy surface and in the solution. Nevertheless, the CR readings dropped when the inhibitor (GOPT) was present. The value was less than 85 mV when the inhibitor was not present. The inhibitor functions as a mixed inhibitor.

Additionally, the unstable values of βa and βc show that corrosion is suppressed while the alloy's anodic dissolving process and hydrogen evolution are uncontrolled. Direct blocking response is used in the inhibition process. The inhibitor (C1025) was physically adsorbed, as indicated by Table 3, which shows that the inhibition efficiency (%E) decreases from 298 to 328 K as the temperature rises [35-39]. When plotting the relationship between ln CR/T versus 1/T, with a slope of $-\Delta H^*/R$ and an intercept of ln R/Nh + $\Delta S^*/R$. The E_a is higher when the inhibitor is present than when it is not, as seen by the rise in the energy barrier in Table 4. Our study's E_a values were consistently below the 80 kJ/mol threshold, which is typically associated with physical adsorption. This suggests that the GOPT inhibitor primarily interacts with the carbon steel surface through physisorption mechanisms. Compared to the blank

Table 3. Tafel parameters for carbon steel 0.1 M HCl in the absence and presence of GOPT at different temperatures

Compound	Conc. (ppm)	T (K)	E_{corr} (mV)	I_{corr} (μA/cm^2)	CR (mpy)	Ba (mV)	Bc (mV/de)	Rp (Ω.cm^2)	%IE	θ
HCl	blank		−611	1092.0	505.500	215.00	−240.20	16.500	-	-
	3		−715	229.3	106.200	422.11	−490.65	78.485	79.00	0.790
	6		−630	220.0	101.620	444.64	−456.06	82.025	80.00	0.800
GOPT	9	298	−638	152.6	70.684	329.96	−715.84	117.920	86.00	0.860
	12		−619	131.4	60.868	215.73	−434.27	136.940	88.00	0.880
	15		−630	124.6	57.718	242.59	−621.55	144.420	88.60	0.886
HCl	blank		−620	1196.0	553.530	249.49	−248.25	15.059	-	-
	3		−597	812.0	376.060	287.98	−326.95	22.165	32.06	0.320
	6	308	−596	668.0	309.350	320.88	−367.34	26.945	44.11	0.440
GOPT	9		−620	665.0	308.060	230.21	−344.17	27.057	44.34	0.444
	12		−619	624.0	288.790	225.75	−405.97	28.863	47.82	0.480
	15		−620	471.0	217.970	245.73	−521.37	38.240	60.62	0.600
HCl	blank		−599	1327.0	614.180	231.00	−259.90	13.571	-	-
	3		−603	851.0	394.280	225.35	−235.06	21.141	35.80	0.358
	6	318	−619	798.0	369.690	241.90	−316.16	22.547	39.80	0.398
GOPT	9		−598	775.0	359.010	316.76	−360.75	23.217	41.55	0.416
	12		−626	609.0	281.950	273.22	−444.54	29.563	54.09	0.541
	15		−593	591.0	273.690	295.09	−342.44	30.455	55.44	0.554
HCl	blank		−614	1359.0	629.030	242.06	−366.58	13.251	-	-
	3		−670	998.0	462.340	445.02	−537.26	18.029	26.50	0.265
	6	328	−611	703.0	325.500	436.06	−540.06	25.608	48.25	0.483
GOPT	9		−604	673.0	311.500	132.86	−168.10	26.795	50.50	0.505
	12		−590	587.0	271.610	249.45	−303.83	30.689	56.82	0.568
	15		−609	470.0	217.440	173.45	−415.21	38.333	65.40	0.654

Table 4. Kinetic parameters for carbon steel of GOPT in 0.1 M HCl at different concentrations

Conc. (ppm)	E_a* (kJ/mol)	ΔH* (kJ/mol)	Δs* (J/mol K)	ΔG* (kJ/mol)			
				328 K	318 K	308 K	298 K
Blank	6.20	3.62	−180.95	57.53	59.33	61.15	62.95
3	36.80	34.20	−88.77	60.63	61.51	61.87	63.30
6	30.45	27.85	−110.38	60.74	61.85	62.95	64.05
9	38.21	35.62	−86.90	61.51	62.39	63.25	64.12
12	37.10	34.48	−91.40	61.71	62.63	63.54	64.45
15	35.00	32.37	−99.30	61.69	62.96	63.94	64.94

solution, the increase in E_a values in the presence of the inhibitor confirms that the inhibitor raises the energy barrier for corrosion, thereby slowing the reaction rate. The positive values of ΔH* observed in Table 4 further indicate that the corrosion process is endothermic. Notably, ΔH* is higher when GOPT is used, reinforcing its role in hindering corrosion. This aligns with the observed increase in CR at elevated temperatures, as thermal input typically favors endothermic reactions.

Additionally, the calculated ΔS* values were significantly negative, indicating a decrease in disorder at the metal–solution interface during inhibitor adsorption. This is likely due to the formation of an organized protective film as GOPT molecules displace water from the metal surface. The ΔG* values, which were more positive in the presence of GOPT, suggest a non-spontaneous corrosion process under inhibitor conditions—further evidence of the inhibitor's effectiveness. These thermodynamic parameters collectively support the conclusion that GOPT adsorbs physically onto the carbon steel surface, reducing corrosion through a barrier mechanism [40-41]. Adsorption equations provide essential details about the interaction between the inhibitor and the carbon steel alloy surface. The Temkin, Frumkin, Freundlich, and Langmuir adsorption equations were used in this research; the latter is considered the most appropriate for GOPT [41]. Since the Langmuir isotherm is the most effective model for obtaining a correlation coefficient (R^2) at or close to one, it was used as the inhibitor in this investigation. Eq. (6) was used to determine the Langmuir isotherm [42];

$$\frac{C_{inh}}{\theta} = \frac{1}{K_{ads}} + C_{inh} \quad (6)$$

where C_{inh} is the concentration inhibitor in ppm, K_{ads} is the equilibrium constant of the adsorption process, and θ is the surface area coverage of a metal surface by C1025 alloy.

The Langmuir adsorption isotherm provided R^2 values almost equal to one in Table 5, making it the best-fitting isotherm for these inhibitors–plot of C_{inh}/θ vs. C at 298 K. As shown in Fig. 7, C_{inh} provides a straight line (K_{ads}) at different temperatures of 308–328 K based on the inverse of the intercept. Eq. (6) was also used to calculate K_{ads} [43-44]. The equilibrium constant of the adsorption

Table 5. Langmuir adsorption isotherm

Conc. (ppm)	C/θ	Temp (K)	R^2
3	3.80		0.99855
6	7.50	298	
9	10.47		
12	13.64		
15	16.93		
3	9.40	308	0.91140
6	13.64		
9	20.30		
12	25.00		
15	25.00		
3	8.40	318	0.92194
6	15.08		
9	21.64		
12	22.20		
15	27.08		
3	11.32	328	0.95499
6	12.42		
9	17.82		
12	21.13		
15	23.30		

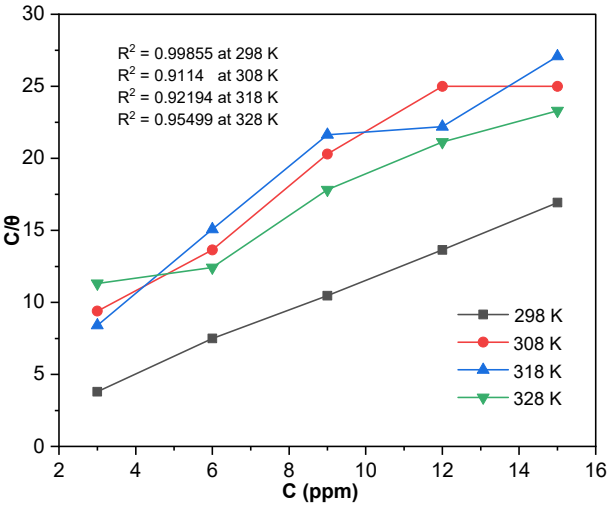

Fig 7. Langmuir's adsorption isotherm

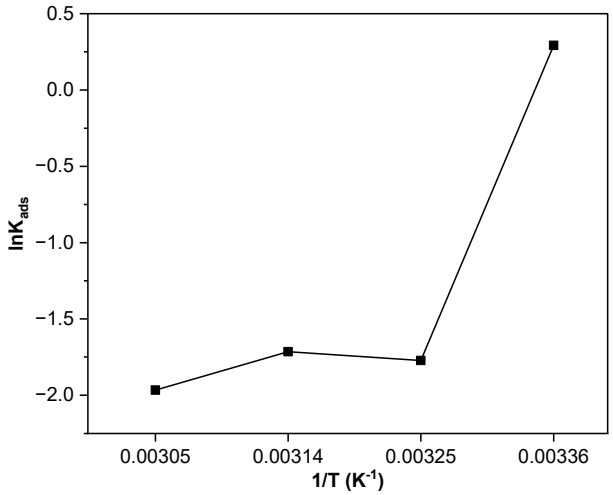

Fig 8. Calculation of ΔH° and ΔS° for the adsorption process

Table 6. Thermodynamic parameters for the adsorption of GOPT on the carbon steel surface in 0.1 M HCl at different temperatures

Comp	Temp (K)	K_{ads} (L/mg)	ΔG° (kJ/mol)	ΔS° (J/mol.K)	ΔH° (kJ/mol)
GOPT	298	1.34	−10.68	−151	−55.68
	308	0.17	−5.75	−162	
	318	0.18	−6.09	−156	
	328	0.14	−5.60	−153	

process should be determined using Langmuir's adsorption isotherms for each inhibitor to calculate the thermodynamic functions of adsorption (e.g., enthalpy, entropy, and free energy of adsorption). Therefore, Eq. (7) can be used to calculate the Gibbs free energy of adsorption;

$$\Delta G^{\circ}_{ads} = -RT\ln(55.5)K_{ads} \quad (7)$$

where, the constant value 55.5 represents the water concentration in a solution in mol/L. Eq. (8) determines the adsorption enthalpy (ΔH°_{ads}) values of the inhibitor (GOPT) [19].

$$\ln K_{ads} = constant - \left(\frac{\Delta H^{\circ}_{ads}}{R}\right)\left(\frac{1}{T}\right) \quad (8)$$

By plotting in Fig. 8, $\ln K_{ads}$ vs. $\frac{1}{T}$, a straight line was obtained, and the given slope is $\frac{-\Delta H^{\circ}_{ads}}{R}$. Furthermore, the entropy of adsorption (ΔS°_{ads}) is calculated according to Eq. (9) [31].

$$\Delta S^{\circ}_{ads} = \frac{\Delta H^{\circ}_{ads} - \Delta G^{\circ}_{ads}}{T} \quad (9)$$

Because the adsorbed layer on the carbon steel surface is stable and the values of ΔG°_{ads} are negative, the results in Table 6 indicate that the adsorption process is spontaneous. When ΔG°_{ads} is less than −40 kJ/mol, the inhibitor (GOPT) is physically adsorbed on the alloy's surface [45-46]. While the ΔH°_{ads} value of the inhibitor (GOPT) is negative; it is a physical adsorption type because it is less than −100 kJ/mol. If ΔS°_{ads} values of inhibitor (GOPT) at different temperatures are negative; these values refer to reducing the disorder between the inhibitor molecule and the corrosive products combined to adsorb on the surface of carbon steel, where these adsorbed constituents tend to associate instead of dissociate to form the activated complex which is the rate-determining step [41].

■ CONCLUSION

As the concentration of GOPT increases, the results show that the novel synthesized chemical inhibitor GOPT is highly effective in controlling the

corrosion of carbon steel alloy (C1025). Moreover, the inhibition efficiency improves with increasing temperature, indicating its suitability for industrial applications under high-temperature conditions, such as in the oil and gas and chemical industries, where equipment protection is crucial. Electrochemical studies revealed that GOPT functions as a mixed-type inhibitor, influencing both anodic and cathodic reactions. Thermodynamic analysis indicated that the adsorption mechanism of GOPT on the carbon steel surface is primarily physical. Based on these findings, GOPT can be considered an effective corrosion inhibitor for carbon steel in acidic environments, particularly under harsh industrial conditions and elevated temperatures, enhancing its potential for practical application in protecting metallic infrastructure.

■ ACKNOWLEDGMENTS

My gratitude goes out to the Iraqi Ministry of Education for providing support. I'd particularly like to thank Dr. Ghassan F. Mohsin for providing me with advice.

■ CONFLICT OF INTEREST

There is no conflict of interest known to be declared.

■ REFERENCES

[1] Bouammali, H., Abrigach, F., Jerdioui, S., El-Haitout, B., Aouniti, A., Touzani, R., Hammouti, B., and Salghi, R., 2024, Effect of the addition of two pyrazole derivatives on the behavior of the corrosion of mild steel in a 1 M HCl medium using experimental and theoretical insights, *Int. J. Corros. Scale Inhib.*, 13 (1), 367–396.

[2] Setti, N., Barrahi, A., Maatallah, M., Kaddouri, Y., Hadda, T., Outada, H., Thakur, A., Touzani, R., Karrouchi, K., Abuelizz, H.A., Dikici, B., Zarrouk, A., and Dafali, A., 2025, Experimental and computational approach on the corrosion inhibition properties of two newly pyrazole derivatives on carbon steel in acid medium, *Sci. Rep.*, 15 (1), 3631.

[3] Mohammed, R.A., and Hussein, S.Z., 2024, Corrosion inhibition of carbon steel in saline water using an azo dye at various concentrations, *Int. J. Corros. Scale Inhib.*, 13 (1), 241–253.

[4] Naser, A.N., Hammed, H., Alshemari, A.Z., and Çardakli, İ.S., 2024, Corrosion inhibitors for carbon steel in HCl environment: Synthesis and characterization of trimethoprim-metal complexes, *Mater. Sci.*, 30 (3), 319–326.

[5] Emil, A.A., Zaur, Z.A., Durna, B.A., and Vasif, B.A., 2024, A systematic review of corrosion inhibitors in marine environments: Insights from the last 5 years, *Processes Petrochem. Oil Refin.*, 25 (3), 793–843.

[6] Senthooran, R., Revon, M.H.N., and Priyantha, N., 2025, Cinnamon leaf extract as an effective inhibitor for mild steel corrosion in pickling bath environments, *Discover Chem.*, 2 (1), 18.

[7] Mustafa, F.A., Saki, T.A., and Hadi, Z.M., 2025, Assessment of boron-modified semicarbazide and thiosemicarbazide resins as corrosion inhibitors for carbon steel alloy in acidic environment, *Samarra J. Pure Appl. Sci.*, 7 (1), 102–123.

[8] AlGhamdi, J.M., Haladu, S.A., Mu'azu, N.D., Alqahtani, H.A., Zubair, M., Manzar, M.S., Alkhowildi, F.A., Kuban, R.Z.M., and AlSubaie, N.F., 2024, Polyethyleneglycol bisphenol A epichlorohydrin copolymer (PEG-BEC) as a highly efficient inhibitor for mild steel corrosion in 1M HCl solutions, *S. Afr. J. Chem. Eng.*, 49, 326–338.

[9] Shwetha, K.M., Praveen, B.M., and Devendra, B.K., 2024, A review on corrosion inhibitors: Types, mechanisms, electrochemical analysis, corrosion rate and efficiency of corrosion inhibitors on mild steel in an acidic environment, *Results Surf. Interfaces*, 16, 100258.

[10] Gaber, G.A., Mohamed, L.Z., and Abd El-Aziz Mohamed, G.H., 2025, Enhancing corrosion behavior of T91 steel in 3.5% NaCl through graphene oxide nanocomposite Coatings, *Egypt. J. Chem.*, 68 (2), 75–89.

[11] Hithesh, M.C., Mohana, K.N.S., Harsha, Y.M., Sreelakshmi, M., and Nayak, S.R., 2025, Development of anti-corrosion coating material by inducting functionalized graphene oxide into

acrylated glucose - vinyl acetate copolymer, *Colloids Surf., A*, 715, 136622.

[12] Mohamed, E.A., Altalhi, A.A., Amer, A., Negm, N.A., Azmy, E.A.M., and Farag, A.A., 2023, Two novel Schiff bases derived from 3-amino-1,2,4-triazole as corrosion inhibitors for carbon steel pipelines during acidizing treatment of oil wells: Laboratory and theoretical studies, *Energy Sources, Part A*, 45 (2), 3246–3265.

[13] Gaber, G.A., Mohamed, L.Z., Aly, H.A., and Hosny, S., 2024, Corrosion potential and theoretical studies of fabricated Schiff base for carbide austempered ductile iron in 1M H_2SO_4 solution, *BMC Chem.*, 18 (1), 170.

[14] Kianfar, M., Seyed Dorraji, M.S., Rasoulifard, M.H., Rahimi, A., and Rahmani, S., 2024, Synthesis and application of aromatic Schiff base waterborne polyurethane as visible-light triggered self-healing polymer and anticorrosion coating using h-BN/GO/NiO nano-composite, *Polym. Test.*, 141, 108649.

[15] Yousif, Q.A., Abdel Nazeer, A., Fadel, Z., Al-Hajji, L.A., and Shalabi, K., 2024, Design of new ecofriendly Schiff base inhibitors for carbon steel corrosion protection in acidic solutions: Electrochemical, surface, and theoretical studies, *ASC Omega*, 9 (12), 14153–14173.

[16] Jafari, H., Ameri, E., Soltanolkottabi, F., and Berisha, A., 2024, Three new reduced forms of synthesized Schiff bases as potent anticorrosion inhibitors for carbon steel in artificial seawater, *J. Mater. Sci.: Mater. Eng.*, 19 (1), 33.

[17] Afshari, F., Ghomi, E.R., Dinari, M., and Ramakrishna, S., 2023, Recent advances on the corrosion inhibition behavior of Schiff base compounds on mild steel in acidic media, *ChemistrySelect*, 8 (9), e202203231.

[18] Saha, S.K., Dutta, A., Ghosh, P., Sukul, D., and Banerjee, P., 2015, Adsorption and corrosion inhibition effect of Schiff base molecules on the mild steel surface in 1 M HCl medium: A combined experimental and theoretical approach, *Phys. Chem. Chem. Phys.*, 17 (8), 5679–5690.

[19] Naser, A.A., Al-Mubarak, A.S., and Al-Sawaad, H.Z., 2019, Synthesis, characterization and evaluation of some graphene oxide derivatives and their application as corrosion inhibitors for carbon steel alloy type C1025 in hydrochloric acid, *Int. J. Corros. Scale Inhib.*, 8 (4), 974–997.

[20] Kumar, A., Verma, S., and Pathak, D.D., 2021 Synthesis and characterization of a recyclable graphene oxide-surface- engineered copper(II) Schiff base complex: Catalytic application in synthesis of 1,2,3-triazoles and 2*H*-indazoles, *J. Environ. Chem. Eng.*, 9 (4), 105791.

[21] Naser, A.A., 2025, Synthesis, characterization, and theoretical analysis of Schiff base graphene oxide utilizing DFT computing, *Acad. Open*, 10 (1), 6–14.

[22] Musthafa Kani, S., Anwar Sathiq, M., and Syed Abuthahir, S.S., 2025, Corrosion resistance properties of expired granisetron drug as an inhibitor for mild steel in 1 M HC, *Port. Electrochim. Acta*, 43, 37–54.

[23] Hamza, S.F., Shahen, S., Abdel-karim, A.M., El-Rashedy, A.A., and Hyba, A.M., 2025, Eco-friendly corrosion inhibitor chitosan methionine for carbon steel in 1 M hydrochloric acid solution: Experimental and theoretical approach, *Sci. Rep.*, 15 (1), 15924.

[24] Al-Qudah, M.A., Bataineh, T.T., Abu Orabi, F.M., Abu-Orabi, S.T., Al-Mazaideh, G.M., and Alakhras, A.I., 2025, Acteoside: A novel green inhibitor for the corrosion of copper in 1.0 M HNO_3 solution: Experimental and theoretical investigation, *RSC Adv.*, 15 (12), 9335–9347.

[25] Naser, A.A., Al-Sawaad, H.Z., and Al-Mubarak, A.S., 2020, Novel graphene oxide functionalization by urea and thiourea, and their applications as anti-corrosive agents for carbon steel alloy in acidic medium, *J. Mater, Environ. Sci.*, 11 (3), 404–420.

[26] Sharma, S., Meena, M., Sharma, H., Yadav, D.K., Tiwari, A., and Verma, V.P., 2022, Fe_3O_4-supported sulfonated graphene oxide as a green and magnetically separable nanocatalyst for synthesis of 2-amino-3-cyano-4*H*-chromene derivatives and them *in-silico* studies, *Synth. Commun.*, 52 (19-20), 1926–1955.

[27] Kumari, S., Shekhar, A., and Pathak, D.D., 2016, Synthesis and characterization of a Cu(II) Schiff base complex immobilized on graphene oxide and its catalytic application in the green synthesis of propargyl amines, *RSC Adv.*, 6 (19), 15340–15344.

[28] Lai, L., Chen, L., Zhan, D., Sun, L., Liu, J., Lim, S.H., Poh, C.K., Shen, Z., and Lin, J., 2011, One-step Synthesis of NH_2-graphene from *in situ* graphene-oxide reduction and its improved electrochemical properties, *Carbon*, 49 (10), 3250–3257.

[29] Naser, A.A., Al-Sawaad, H.Z., and Al-Mubarak, A.S., 2020, Phosphorous acid functionalized graphene oxide by microwave and evaluation as anticorrosion inhibitor for carbon steel alloy type C1025 in HCl solution, *J. Kufa Chem. Sci.*, 2 (6), 145–165.

[30] Motameni, A., Alshemary, A.Z., Dalgic, A.D., Keskin, D., and Evis, Z., 2022, Graphene oxide reinforced doped dicalcium phosphate bone cement for bone tissue regenerations, *J. Aust. Ceram. Soc.*, 58 (5), 1633–1647.

[31] Mohsin, G.F., and Alzubaidi, A.K., 2023, The influence of pH and molar ratio on melanoidin skeleton formation, *Food Res.*, 7 (5), 97–102.

[32] Mohsin, G.F., Al-Kaabi, W.J., and Alzubaidi, A.K., 2022, Describing Polymers synthesized from reducing sugars and ammonia employing FTIR spectroscopy, *Baghdad Sci. J.*, 19 (6), 1297–1304.

[33] Eftekhar, M., and Raoufi, F., 2022, Synthesis, characterization and first application of graphene oxide functionalized Cu(II) complex for the synthesis of 1,2,3-triazole derivatives, *Polycyclic Aromat. Compd.*, 42 (7), 4780–4792.

[34] Myasoedova, T.N., Nedoedkova, O.V., and Yalovega, G.E., 2024, Electrophysical properties of composite materials based on graphene oxide and polyaniline, *Kondens. Sredy Mezhfaznye Granitsy*, 26 (1), 104–110.

[35] Manssouri, M., El Ouadi, Y., Znini, M., Costa, J., Bouyanzer, A., Desjobert, J.M., and Majidi, L., 2015, Adsorption proprieties and inhibition of mild steel corrosion in HCl solution by the essential oil from the fruit of Moroccan *Ammodaucus leucotrichus*, *J. Mater. Environ. Sci.*, 6 (3), 631–646.

[36] Elkhotfi, Y., Forsal, I., Rakib, E.M., and Mernari, B., 2018, The inhibition action of essential oil of *Juniperus phoenicea* on the corrosion of mild steel in acidic media, *Port. Electrochim. Acta*, 36 (2), 77–87.

[37] Obaid, H.T., Kadhum, M.Y., and Abdulnabi, A.S., 2022, Azo Schiff base derived from 2-hydroxy-1-naphthaldehyde as corrosion inhibitors for carbon steel in HCl medium: Experimental and theoretical, *Mater. Today: Proc.*, 60 (Part 3), 1394–1401.

[38] Al-Jubanawi, I.M., Al-Sawaad, H.Z., and AlWaaly, A.A., 2020, Bis thiourea phthalate cobalt(II) complex: Synthesis and studying as corrosion inhibitors for carbon steel alloy (C1010) in 0.1 M HCl, *J. Mater. Environ. Sci.*, 11 (8), 1386–1402.

[39] Alhijaj, H.A.A., 2015, Synthesis and Characterization of Polymeric Compounds from Waste Polyethylene Terephthalate and Polystyrene and Studying its Efficiencies as Oil Spill Cleanup and Corrosion Inhibitors, *Dissertation*, Department of Chemistry, College of Science, University of Basrah, Iraq.

[40] Mohammed Ali Al-Sammarraie, A., and Hasan Raheema, M., 2017, Electrodeposited reduced graphene oxide films on stainless steel, copper, and aluminum for corrosion protection enhancement, *Int. J. Corros.*, 2017 (1), 6939354.

[41] Ali, A.N., 2020, Synthesis of Graphene Oxide and Some of Its Functionalized Derivatives and their Evaluation as Corrosion Inhibitors for Carbon Steel C1025 Alloy in HCl Solution, *Dissertation*, Department of Chemistry, College of Science, University of Basrah, Iraq.

[42] Khelfaoui, M., Zouied, D., Bouzenad, N., Abdennouri, A., Boussouf, I., Damous, M., Boucetta, R.N., Merzeg, F.A., Djermoune, A., and Belhocine, Y., 2025, Antimicrobial activity and high anticorrosion efficiency of *Carpobrotus acinaciformis* L. extracts against C1020 carbon steel corrosion in a hydrochloric acid medium, *Chem. Biochem. Eng. Q.*, 39 (1), 15–28.

[43] Layla, A.J., 2016, Polyvinyl pyrrolidone as a corrosion inhibitor for carbon steel in HCl, *Int. J. Electrochem. Sci.*, 11 (3), 2247–2262.

[44] Benchadli, A., Attar, T., Messaoudi, B., and Choukchou-Braham, E., 2021, Polyvinylpyrrolidone as a corrosion inhibitor for carbon steel in a perchloric acid solution: Effect of structural size, *Hung. J. Ind. Chem.*, 49 (1), 59–69.

[45] Lebrini, M., Robert, F., and Roos, C., 2013, Adsorption properties and inhibition of C38 steel corrosion in hydrochloric solution by some indole derivates: Temperature effect, activation energies, and thermodynamics of adsorption, *Int. J. Corros.*, 2013 (1), 139798.

[46] Ojo, F.K., Adejoro, I.A., Lori, J.A., Oyeneyin, O.E., and Akpomie, K.G., 2022, Indole derivatives as organic corrosion inhibitors of low carbon steel in HCl medium-experimental and theoretical approach, *Chem. Afr.*, 5 (4), 943–956.